Flow Characteristics of Laminar Separation on Surface-Mounted Ribs

Shou-Shing Hsieh*
National Sun-Yat Sen University, Koahsiung, Taiwan
and
Durn-Yuan Huang†
National Koahsiung Institute of Technology, Koahsiung, Taiwan

The fluid flow characteristics of steady-state laminar flow over surface-mounted ribs was studied using the SIMPLE/HD finite-difference numerical scheme with uniform/nonuniform grid systems. Grid dependence of uniform/nonuniform systems was examined. Pressure and velocity distributions were obtained to define the pressure and friction coefficients. It appears that the variation of Reynolds number and the rib width-to-depth ratio is of significance on total drag and, finally, it is correlated in the form of $C_d = 0.127\,(Re_s)^{0.39}(w/s)^{0.03}$ for $1 \le w/s \le 4$, and $63.5 \le Re_s \le 254$. The results may provide further insight regarding flow behavior near rib-type roughened surfaces and have application to engineering problems.

Nomenclature

C_d	= total drag coefficient
C_p	= static pressure coefficient, $C_p = \Delta p / \frac{1}{2}\rho u_\infty^2$
L_r	= reattachment length
L_u, L_d	= length of upstream and downstream boundaries, respectively
p	= pressure
p_0, p_∞	= pressure at inlet and freestream pressure, assumed zero for present study
Δp	$= p - p_\infty$
U_∞	= freestream velocity
s	= rib depth
u, v	= velocity in x and y directions, respectively
w	= rib width
x	= downstream distance
ρ	= density
μ	= viscosity
δ	= boundary-layer thickness

Subscripts

d	= drag
p	= pressure
r	= reattachment
s	= rib height
∞	= freestream
0	= inlet

Introduction

A DISTRIBUTION of roughness elements along an otherwise smooth wall boundary surface can significantly alter the dynamic processes of the flow. In laminar flows, which are relatively stable, such alterations cause little or no change in the surface drag along these surfaces. In turbulent flows, such alterations, in general, cause a surface drag increase and the flow/surface interaction is rather complex due to the broad spectrum of dynamically relevant scales of motion present in the flow. Initially, it is necessary to treat a more tractable flow situation that incorporates the important parameters and features of the flow. The two-dimensional laminar boundary-layer flow over surface-mounted ribs constitutes such a first approximation. The objective of this study is to gain detailed insight into the dynamics of such flows.

A number of experimental studies of boundary-layer flows (either external or internal) over surface-mounted ribs, several of which were turbulent, have focused on the overall features of the flow, such as velocity and surface pressure distributions and skin-friction variations.[1-6] There have also been numerical studies[7-9] of the flow past a bluff body similar to the present investigation. These studies have been limited to high-speed flows and do not provide the insight required in the present paper. The intent here is to provide flow characteristics over a range of rib sizes in terms of the variation of the rib width-to-depth ratio (w/s) and Re at relatively low speed near the wall environment, which is typical of the local conditions for roughness elements.

The present calculations are performed using the well-known SIMPLE/HD numerical scheme. The conventional methodology for solving the equations of motion, expressed in terms of primitive variables u, v, and p in conjunction with uniform and nonuniform grid systems, was applied to the present problem. Velocity profiles and boundary-layer reattachment length, as well as wall static pressure coefficients in the vicinity of the rib were generated to permit a detailed study of laminar flow over surface-mounted ribs. The pressure-induced forces on the vertical walls of the rib, which are important in the overall drag characteristics was calculated. Finally, total drag values are extracted from the computed results. Another important feature of the results is the fact that a considerable reduction of the computation time could be achieved if a nonuniform mesh system is properly chosen.

Method of Analysis

The governing equations for steady-state laminar flow can be written with constant properties as:

Continuity:

$$\frac{\partial u}{\partial x} + \frac{\partial v}{\partial y} = 0 \tag{1}$$

X momentum:

$$\rho\left(u\frac{\partial u}{\partial x} + u\frac{\partial u}{\partial y}\right) = \mu\left(\frac{\partial^2 u}{\partial x^2} + \frac{\partial^2 u}{\partial y^2}\right) - \frac{\partial p}{\partial x} \tag{2}$$

Received Feb. 12, 1986.

*Associate Professor, Department of Mechanical Engineering. Member AIAA.
†Instructor, Department of Die Engineering.

Y momentum:

$$\rho\left(u\frac{\partial v}{\partial x}+u\frac{\partial v}{\partial y}\right)=\mu\left(\frac{\partial^2 v}{\partial x^2}+\frac{\partial^2 v}{\partial y^2}\right)-\frac{\partial p}{\partial y} \tag{3}$$

The form of calculation domain is shown in Fig. 1. It will be found later that the dividing streamline shown in the figure is correct for this study. The inlet boundary AB is located by trial and error sufficiently upstream of the obstacle so that its presence is not felt and the outlet is located sufficiently downstream of the point of reattachment. The lower boundary corresponds to the solid wall and the upper boundary corresponds to the free boundary. The values of the various dimensions and boundary conditions are given for each case in Table 1. Nonslip boundary conditions are imposed along the walls and zero normal gradients are given at the outlet plane and along the free boundary. At inlet plane AB, a result from laminar boundary-layer profile for a smooth wall is imposed on axial velocity. In summary, the velocity and pressure boundary conditions are indicated in Table 2.

Figure 2 shows a two-dimensional staggered grid pattern, with the locations for u, v, and p placed on the respective control volume faces. This can also be seen in Fig. 2 for each staggered control volume for u, v, and p. The usual finite-volume process of integrating Eqs. (2) and (3) over the control volume at each node and introducing suitable centered approximations for the diffusion terms was made to obtain the simultaneous algebraic equations.

A conventional numerical scheme with uniform (48×80) and nonuniform (30×54) grids, of which detailed illustrations are shown in Fig. 3, was chosen to apply to the present physical system. The dimension of uniform grid is 0.2 s. For nonuniform grid, the finest grid (of dimension 0.025 s) is located adjacent to the wall and the sizes of other grids are chosen such that each is within 125% of adjacent grids in order to avoid abrupt changes and to obtain convergence.

The calculation are started at a distance of two rib heights upstream of the rib. Downstream of the rib, the grids are extended a maximum distance of 11 rib heights. The calculation domain in the y direction is up to a distance sufficient to make sure that, for the smallest value of the Reynolds number, the plane BC in Fig. 1 lies well outside of the boundary layer specified on plane AB. In the present study, locating plane BC at a distance of 9.5 times the rib height above the wall has been found to be sufficient.

The numerical procedure used is based on the iterative scheme. This procedure used the hybrid central/upwind difference scheme for the convective terms with central difference for the diffusion terms. For the convective terms, upwind difference is used if the grid Peclet number in a given direction is greater than 2. When the grid Peclet number is less than or equal to 2, central difference is employed. This procedure incorporates the SIMPLE solution technique initiated by Patankar and Spalding,[10] which is based on the solution of the difference equations obtained by integrating the differential equations for momentum over the control volume enclosing the nodal points. The solution of the set of difference equations over the entire region of the interest is obtained by evaluating new values for any desired variable, taking into account the latest known estimated value of the variable on the

Table 1 Geometrical parameters

Parameters	Rectangular rib Uniform (40×80)/Nonuniform (30×54)
s	Height of rib
w	Width of rib
H	9.5S
L_u	2S
L_d	$\geq$13.7S
Top boundary	Free
$U\infty$	10, 20, 40 cm/s
δ	2.6, 1.839, 1.3 cm
w/s	1, 2, 4
Re_s	63.5, 127, 254

Table 2 Boundary conditions for numerical calculations

1) On solid boundaries:	3) On plane BC:
$u=0,\ v=0$	$\frac{\partial u}{\partial y}=0,\ \frac{\partial v}{\partial y}=0$
2) On plane AB:	4) On plane CD:
$p_0=0,\ v=0$	$\frac{\partial u}{\partial x}=0,\ \frac{\partial v}{\partial x}=0$
$u=u(y)$ specified	

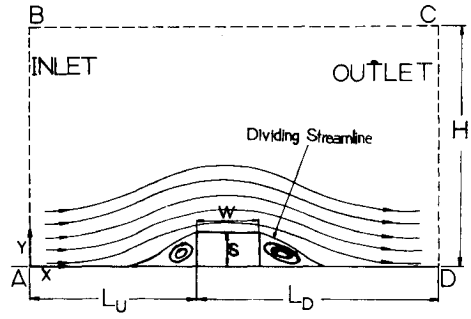

Fig. 1 Schematic of domain of calculations.

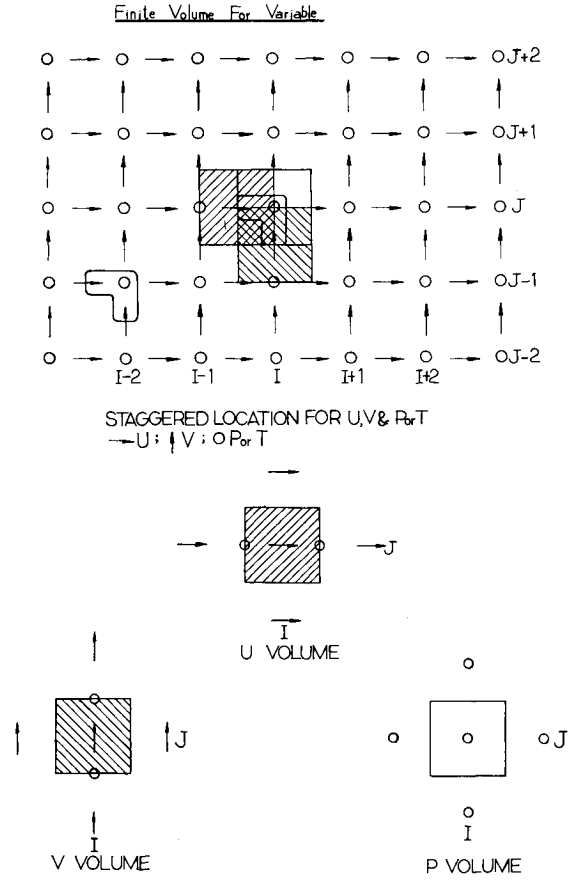

Fig. 2 Finite control volume representation.

neighboring nodes. One iteration of the solution is completed when, in a line-by-line technique, all of the lines in a chosen direction have been accounted for. Line inversion iteration with an under-relaxation value of 0.5 for the velocity terms and 0.8 for the pressure correction term was incorporated to speed the calculations.

In the present study, calculations are obtained for $w/s = 1$, 2, and 4. By first assuming a pressure distribution within the calculation domain, the set of difference equations for the x and y momentum is solved by line iteration. After a sweep of the solution domain is completed, adjustments are made to the pressure field so that the continuity and momentum are simultaneously satisfied. The convergence criterion used is that the change in a variable at any node should be less than 0.2%. To validate the numerical scheme utilized in the present study, initial calculations are performed for the laminar flow over a flat plate and flow past a cavity. The testing results agree reasonably well with existing data reported by Bhatti and Aung.[11]

Results and Discussion

Representative computed results for the flowfield are indicated using the case of $w/s = 4$ at two Reynolds numbers. Nondimensional velocity profiles at various axial locations over the rib are shown in Fig. 4. For the two Reynolds numbers shown, the recirculating flow is seen in the upstream and downstream regions of the rib with different maximum reverse flow velocities and reattachment lengths. Important features of this figure are that, for instance, at $Re_s = 127$ the onset of separation takes place at $x/s = 0.6$ and recirculation flow starts. In this region, the maximum reverse velocity is roughly 11% of the freestream value. At the top wall of the rib, the velocity is nearly the same as that of flow over a flat plate. As flow keeps moving downstream, the recirculation occurs again. The maximum reverse velocity is about 2% of the freestream velocity, which is much lower than that of in the upstream region.

For all the calculations of the configurations under consideration, the results show that the onset of separation at high Reynolds numbers occurs earlier than at low Reynolds numbers. However, the reattachment point goes the other way around in the downstream region, which results in a slower recovery of velocity profile at high Reynolds numbers.

Two different grid systems were employed (uniform 48×80 and nonuniform 30×54) and representative results at three locations of $x/s = 1.8$, 4, and 6.4 for upstream recirculation zone, top wall, and downstream recirculation zone are presented in Fig. 5 in the form of velocity profile. It is seen that the solution for the nonuniform grid is to all intents and purposes grid independent.

By closely examining the computed velocity distribution results, the location where the slope of the velocity at the downstream wall equals zero may be ascertained. Figure 6 indicates the normalized reattachment lengths as a function of the Reynolds number (L_r/s, where L_r is measured from corner of the rib on the downstream side). There is considerable scatter in the data, but it is possible to draw a mean straight line through the data. It seems that the reattachment length L_r at

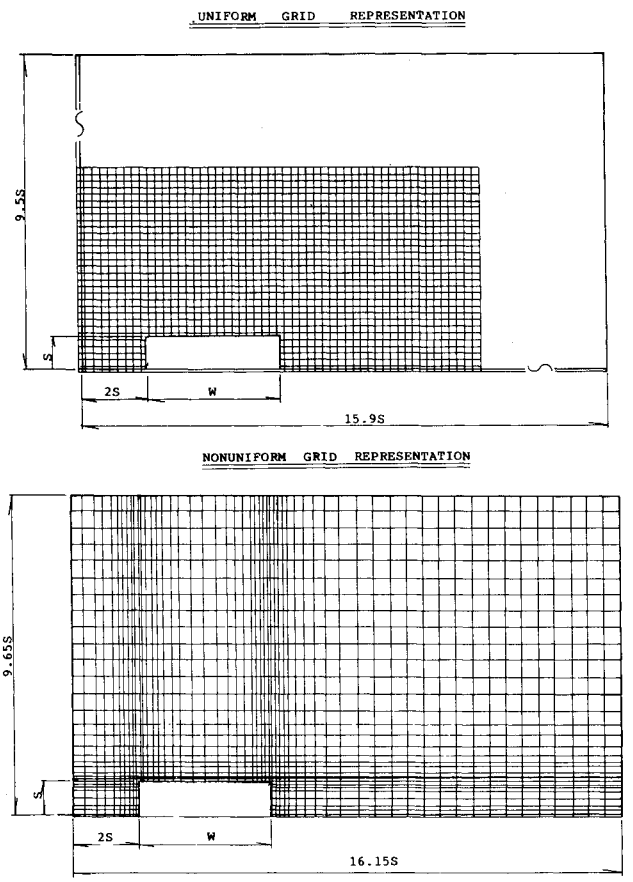

Fig. 3 Uniform and nonuniform grid system.

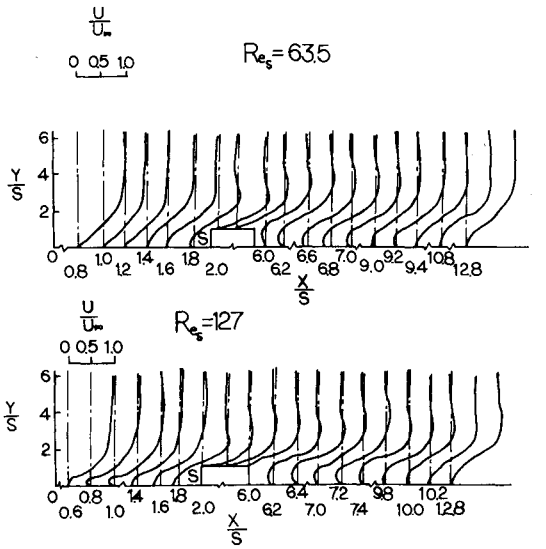

Fig. 4 Velocity distribution at various axial locations for $w/s = 4$.

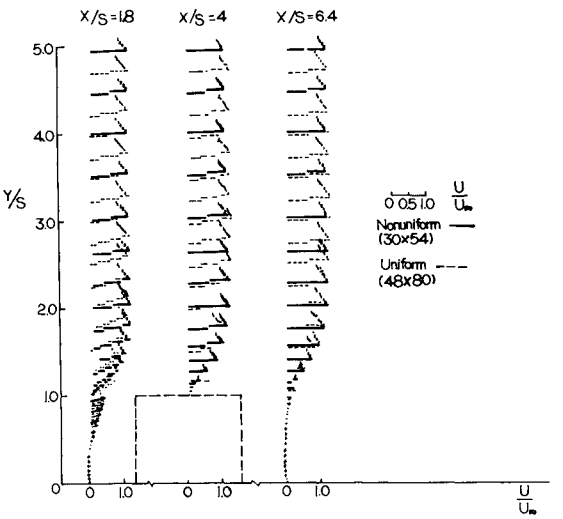

Fig. 5 Uniform and nonuniform dependence of the flowfield at different downstream distances.

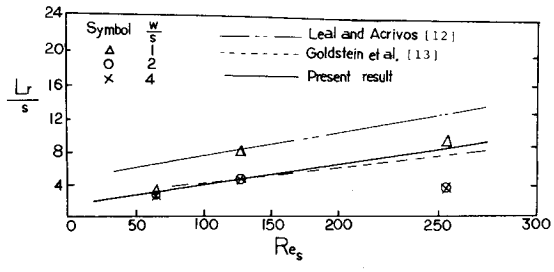

Fig. 6 Reattachment length $L_{r/s}$ vs Re_s.

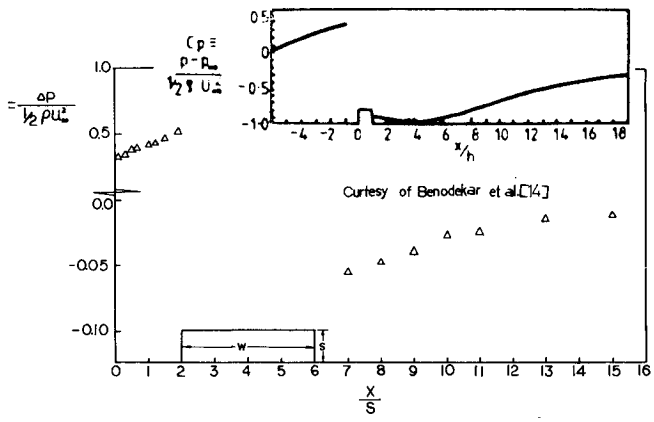

Fig. 7 Typical pressure coefficient distribution for $w/s=4$ and comparison with Ref. 14 results for turbulent flow over a square rib.

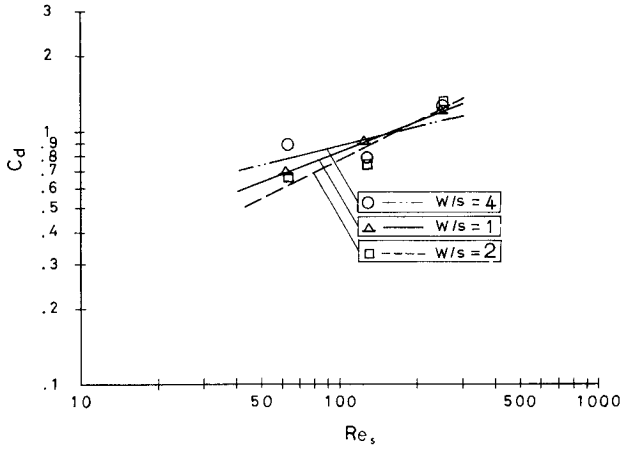

Fig. 8 Dependency of w/s on total drag C_d.

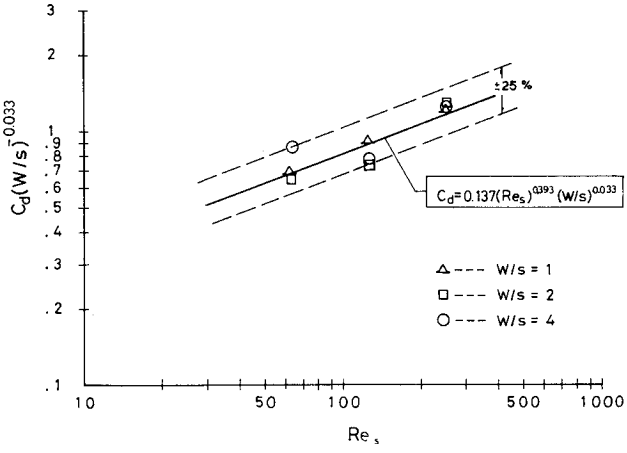

Fig. 9 Analytical correlation of C_d.

$Re_s=127$ and 254 for $w/s=4$ shows a lower value than it should. This underprediction occurs for reasons that are not clearly understood at this stage. But, nevertheless, the present result falls between the data from Leal and Acrivos[12] and Goldstein[13] or relatively unconfined flow past a bluff body, which is encouraging.

In Fig. 7, the calculated wall static pressure distribution is plotted vs downstream distance. This is in agreement with the trend exhibited by the data of Benodekar et al.[14] The discrepancy of the values was expected because the present flow is everywhere laminar, while the work of Benodekar belongs to turbulent flow.

One of the main objectives of the present study was to examine the effects of the rib on total drag. In the absence of the rib, the drag is due solely to skin friction; with the rib, the effects of pressure drag on the vertical walls of the rib must be accounted for in addition to friction drag. As a result, the total drag coefficient close to the rib is plotted against the Reynolds number for all three values of w/s in Fig. 8 and detailed values for each contribution to the total drag coefficient are listed in Table 3. The influence of the parameter w/s can be noted distinctly for the larger width-to-height rato giving the moderate total drag at high Reynolds numbers. The theoretical results are represented by the following equations through least square techniques:

$$C_d=0.153(Re_s)^{0.36} \quad \text{for } w/s=1 \tag{4}$$

$$C_d=0.054(Re_s)^{0.56} \quad \text{for } w/s=2 \tag{5}$$

$$C_d=0.262(Re_s)^{0.26} \quad \text{for } w/s=4 \tag{6}$$

The wide variation of coefficient C and the power of Re for all three rib configurations indicates that a unique analytical approximation having the form of

$$C_d=0.127(Re_s)^{0.393}(w/s)^{0.033}$$

might be possible within a limit of ±25% to the original computed data shown in Fig. 9. It appears that the values of C_d for all rib configurations can be represented by that of the $w/s=1$ case, which can be seen from the power (=0.033) of w/s and the coefficient (=0.127) in this unique correlation by making comparisons with those of Eq. (4).

Table 4 summarizes the number of iterations required to obtain the solutions just discussed. This shows that a suitable nonuniform grid selection is essentially needed as far as the reduction of computation time is concerned. But great care

Table 3 Predicted value of drag coefficient

		Drag coefficient		
Re_s	w/s	Friction	Pressure	Total
63.5	1	0.0932	0.5898	0.6830
	2	0.1440	0.4627	0.6067
	4	0.2186	0.6322	0.8508
127	1	0.0551	0.8131	0.8682
	2	0.0975	0.5945	0.6920
	4	0.1500	0.5898	0.7398
254	1	0.0317	1.0928	1.1245
	2	0.0248	1.2951	1.3199
	4	0.0411	1.1760	1.2171

Table 4 Number of iteration for rectangular ribs

Grid	w/s	Scheme	No. of iteration (approx.)
40×80	4	Uniform	150
30×54	4	Nonuniform	75

should be taken in choosing a suitable mesh in order to avoid additional data distortion caused by an unsuitable nonuniform mesh system.

The present numerical study adequately provides the basic flow patterns for laminar flow over a surface-mounted rib. It would be interesting to see the effect of including the ratio of δ/s in the computation.

Conclusions

The present study is aimed at providing an understanding of the dynamic process of laminar flow over surface-mounted ribs. The detailed investigation conducted here shows that the reattachment length is a function of Reynolds number of the rib (Re_s) and that the nature of the flow in the vicinity of the ribs with laminar separation seems controlled mainly by the variation in the w/s ratios in the absence of the effect of the ratio of δ/s.

The wall static pressure distribution is found to be in good agreement with previous research. It was found the influence of Reynolds number and w/s ratio on the total drag is significant. Thus, the total drag coefficient C_d can be represented in the form of

$$C_d = 0.127 (Re_s)^{0.393} (w/s)^{0.033}$$

in terms of Reynolds number of the rib and the width-to-height ratio for $63.5 \le Re_s \le 254$ and $1 \le w/s \le 4$.

Acknowledgment

The authors wish to thank the computer center staff and computer facility of National Koahsiung Institute of Technology for their assistance throughout the course of the present work.

References

[1]Berner, C., Durst, F., and McEligot, D. M., "Flow Around Baffles," *Journal of Heat Transfer*, Vol. 106, Nov. 1984, pp. 743–749.

[2]Nunner, W., "Heat Transfer and Pressure Drop in Rough Tubes," AERE lib/Trans. 786, 1958.

[3]Good, M. C. and Joubert, P. N., "The Form Drag of Two-Dimensional Bluff Plates Immersed in the Turbulent Boundary Layers," *Journal of Fluid Mechanics*, Vol. 31, Feb. 1968, pp. 547–582.

[4]Han, J. C., "Heat Transfer and Friction in Channels with Two Opposite Rib-Roughened Walls," *Journal of Heat Transfer*, Vol. 106, Nov. 1984, pp. 774–781.

[5]Gee, D. L. and Webb, R. L., "Forced Convection Heat Transfer in Helically Rib-Roughened Tubes," *International Journal of Heat and Mass Transfer*, Vol. 23, 1980, pp. 1127–1136.

[6]Webb, R. L., Eckert, E. R., and Goldstein, R., "Heat Transfer and Friction in Tubes with Repeated-Rib Roughness," *International Journal of Heat and Mass Transfer,* Vol. 14, 1971, pp. 601–617.

[7]Kumur, A. and Yajnik, K. S., "Internal Separated Flows at Large Reynolds Numbers," *Journal of Fluid Mechanics*, Vol. 97, 1980, pp. 27–51.

[8]Eagles, P. M. and Smith, F. T., "The Influence of Nonparallelism in Channel Flow Stability," *Journal of Engineering Mathematics*, Vol. 14, 1980, pp. 219–237.

[9]Gosman, A. D. and Ideriah, F. J. K., "A General Computer Program for Two-Dimensional Turbulent Recirculating Flows," Dept. of Mechanical Engineering, Imperial College, London, 1979, pp. 10.37–10.42.

[10]Patankar, S. V., *Numerical Heat Transfer and Fluid Flow*, Hemisphere Publishing Co., New York, 1980.

[11]Bhatti, A. and Aung, W., "Finite Difference Analysis of Laminar Separated Forced Convection in Cavities," *Journal of Heat Transfer*, Vol. 106, Feb. 1984, pp. 49–54.

[12]Leal, L. G. and Acrivos, A., "The Effect of Base Bleed on the Steady Separated Flow Past Bluff Objects," *Journal of Fluid Mechanics*, Vol. 39, Dec. 1969, pp. 735–752.

[13]Goldstein, R. J., "Laminar Separation, Reattachment and Transition of Flow Over a Downstream Facing Step," *Transactions of ASME, Journal of Basic Engineering*, Ser. D, Vol. 92, Dec. 1970, pp. 732–741.

[14]Benodekar, R. W. et al., "Numerical Prediction of Turbulent Flow over Surface-Mounted Ribs," *AIAA Journal*, Vol. 23, March 1985, pp. 359–366.